Mode I delamination fatigue crack growth in unidirectional fiber reinforced composites: Results from ESIS TC4 round-robins

S. Stelzer[1], A.J. Brunner[2], A. Argüelles[3], N. Murphy[4], G.M. Cano[5], G. Pinter[1,6]

[1] *Institute of Materials Science and Testing of Plastics, Montanuniversität Leoben, Franz-Josef-Strasse 18, A-8700 Leoben, Austria, steffen.stelzer@unileoben.ac.at*

[2] *Empa, Swiss Federal Laboratories for Materials Science and Technology, Überlandstrasse 129, CH-8600 Dübendorf, Switzerland*

[3] *Department of Construction and Manufacturing Engineering, Universidad de Oviedo, Campus de Viesques, Gijón 33203, Spain*

[4] *School of Mechanical and Materials Engineering, UCD Engineering and Materials Science Centre, University College Dublin, Belfield Dublin 4, Ireland*

[5] *Instituto Nacional de Técnica Aerospacial, Carretera de Ajalvir, Km 4, 28850 Torrejón de Ardoz, Spain*

[6] *PCCL, Polymer Competence Center Leoben, Roseggerstrasse 12, A-8700 Leoben, Austria*

Abstract

Two round robins on mode I fatigue delamination propagation organized by Technical Committee 4 of the European Structural Integrity Society compared three unidirectional carbon fiber reinforced composites, one with thermoplastic (poly-ether-ether-ketone) and two with thermoset (epoxy) matrix tested at five laboratories. Different approaches for data evaluation and their effect on the in- and inter-laboratory scatter are discussed and compared. Results are very sensitive to small scatter in the load signal, and, therefore, a new route to evaluate the crack growth rate from pairs of load and displacement data is presented.

Keywords: *Polymer-matrix composites (PMCs); delamination; fatigue; fracture; test development*

1 Introduction

In recent years fiber reinforced polymer composites have gained in importance, especially due to the growing interest of the transportation industry in lightweight structures [1–4]. But notwithstanding their many advantages, the biggest disadvantage of using fiber-reinforced polymer-matrix (FRP) composite materials is their susceptibility to delamination initiation and growth of these interlaminar delaminations (see, e.g., [5, 6] for recent reviews). To account for the need to characterize the delamination resistance of FRPs under monotonic mode I loading conditions a significant research effort was carried out in the last three decades [5–13]. Several research groups have further published results of cyclic mode I delamination measurements on FRP [12, 14–25]. There are approaches for incorporating delamination properties into structural design [26] and quasi-static as well as cyclic fatigue fracture mechanics data from composite laminates have been used to predict the delamination behavior of composite structures [27–31].

Standards considering the determination of the critical value of the interlaminar fracture toughness, G_{IC}, for unidirectionally reinforced polymer composites under quasi-static load were published [32–34]. Furthermore a standard for the measurement of delamination fatigue growth onset was issued in 2008 [35]. Recently, European Structural Integrity Society Technical Committee 4 (ESIS TC4) and American Society for Testing and Materials, International, Subcommittee D30.06 (ASTM D30.06) carried out separate round-robin test programs on mode I (tensile opening) fatigue delamination growth. Selected results and additional references have been compiled in [36–38], but so far no standards considering mode I fatigue crack propagation in unidirectionally reinforced (UD) polymer

composites have been published. The applicability of mode I fatigue test procedures to glass fiber-reinforced polymer-matrix (GFRP) laminates was investigated [22, 27] and it was shown that different types of FRP laminates could be discriminated [37]. The 2009 round robin exercise carried out by ESIS TC4 investigated the influences of control mode (load vs. displacement control), test frequency and test duration on the overall test results [36] performed at three laboratories. None of these test parameters was found to exert a significant influence when testing a carbon fiber reinforced epoxy laminate (IM7/977-2). Selected results from preliminary testing and of a first round robin of ESIS TC4 and ASTM D30.06 published in [38] focused on discrimination between different composite laminates and, in part, on determination of threshold values. A second ESIS TC4 round robin performed in 2010-2011 focused on material dependent inter-laboratory scatter by testing one carbon fiber epoxy laminate (G30-500 12k/R5276) and one carbon-fiber poly-ether-ether-ketone (AS4/PEEK) laminate at five laboratories. Possible sources of inter-laboratory scatter include different types of test machines used at participating laboratories, different test set-ups and frequencies, and different operators recording the visually determined delamination lengths.

Compared with tests described in the literature so far, a round robin with several participating laboratories for the first time allows the determination of inter-laboratory scatter. The in-laboratory scatter can be compared to previously published literature for the same or similar composite laminates. In order to have comparable results, a number of test parameters were prescribed (see below for details).

In order to facilitate testing in an industrial test environment particular emphasis was placed on short test duration and automated data

acquisition [36]. Therefore, threshold determination was not an aim of the round robins. As discussed in [38], threshold value determination may require higher resolution of load and displacement than mode I fatigue delamination propagation. The present paper for the first time compiles all data sets from the mode I fatigue delamination propagation round robins performed within ESIS TC4.

2 Experimental

2.1 Materials and specimens

Three materials, listed in Table 1, were tested within the ESIS TC4 round robin exercises. DCB specimens based on prescriptions and recommendations in [34] with a total length of about 145 mm, a width of 20 mm and thicknesses as listed in Table 1 were used. For starting the crack a poly-tetra-fluoro-ethylene (PTFE) film (about 20 µm thick), inserted at the laminate mid-plane, was used in materials A and B, and a fluorinated ethylene propylene (FEP) film (about 10 µm thick) in material C. [34] recommends the use of film inserts with less than 13 µm thickness in order to simulate a sharp crack. In the ESIS TC4 round robin a monotonic precrack was generated prior to fatigue testing in order to avoid an influence of the film insert on the crack growth. Aluminum load-blocks were mounted for load introduction.

2.2 Procedure

The round robin test procedure and the results presented here are based on the experience from published literature [7–25] and preliminary testing at selected laboratories [37]. The 2011 test procedure in principle allows testing at different stress ratios, R, test frequencies and under load or displacement control. For ease of comparison in the round robin, testing

was limited to displacement control based on a comparison between load and displacement control from the first round robin [36]. Test frequencies shall be chosen as high as possible, but possible heating effects would have to be investigated for frequencies of 10 Hz or higher. Data will be presented as a function of G_{Imax} rather than ΔG for eliminating scatter due to possible facial interference and the prescribed stress ratio of R=0.1 will yield conservative results when using G_{Imax} [14]. Facial interference comprises a combination of effects including fiber bridging (e.g., fibers of both crack faces interfere during the crack closing step), a plasticity zone wake (usually called crack closure in metals), rough surface and debris [18]. The ESIS TC 4 procedure specified that in order to start the measurements at high crack growth rates just below G_{IC}, a quasi-static mode I test for pre-cracking was performed as a G_{IC}-test at a cross-head speed of between 1 and 5 mm/min, ideally to obtain a short, i.e., a few mm long precrack. Cyclic fatigue loading was then started with the last displacement value from the quasi-static test, since choosing a maximum displacement from the average of all quasi-static tests, e.g., according to equation (1) as required by the ASTM D30.06 procedure proved difficult because of the scatter among specimens (mainly due to stiffness variation).

$$\delta_{\max} = \sqrt{\left[0.8 \cdot \delta_{cr}\right]^2_{av}} \qquad (1)$$

where δ_{max} is the maximum displacement in the cyclic test and δ_{cr} is the critical displacement in the quasi-static test. The fatigue tests were continued until a crack growth rate of about 10^{-6} mm/cycle was reached. Fatigue loading could be stopped to perform visual observation of delamination lengths with a travelling microscope. In order to avoid errors

during the calculation of the results a spreadsheet macro file was created which was used by all the participants for the calculation of the so-called Paris plot, i.e., da/dN as a function of G_{Imax}. The tests were carried out in five different laboratories (labeled A,B,C,D,E) using five different test machines. Laboratory A used a servo-hydraulic test machine (type MTS 858) with a 15 kN load cell calibrated to a load range between 0 and 400 N. The tests at laboratory B were done on a servo-hydraulic test machine (type MTS Bionix) with a 15 kN load cell. Laboratory C used a servo-hydraulic test machine (type Instron 1273) with a 1 kN load cell, calibrated to a load range between 0 and 500 N. Laboratory D used a servo-hydraulic test machine (type Instron 8502) with a load cell capacity of 5 kN. Laboratory E carried out the tests on a servo-hydraulic test machine (type Instron 8872) with a 5 kN load cell. Laboratories A and B performed the tests at a maximum frequency of 10 Hz, laboratory C at 3 Hz and laboratories D and E at 5 Hz. Labs A, B and D had to reduce the test frequency when testing the more compliant PEEK specimens due to the greater piston displacement that was needed to keep the interlaminar crack growing.

2.3 Crack length detection

The crack length, a, was determined using three different approaches. All round robin participants used a travelling microscope with a sufficient resolution for visual crack length detection as defined in [34] as first method. Based on these visually observed crack lengths and the corresponding machine data, a compliance based approach (see equation 2) was used as second method to calculate crack lengths from every pair of load and displacement values recorded by the test machine at selected intervals during the test as explained in [36].

$$a = \left(\frac{C}{B} \right)^{\frac{1}{m}} \tag{2}$$

where C is the compliance determined from machine load and displacement and B and m are constants of a power-law fit. Figure 1a shows such a power law fit and Figure 1b the resulting crack length as a function of the number of cycles after applying this compliance calibration to load and displacement data recorded by the test machine.

As third method, the so-called “effective” crack length method can be applied in order to back-calculate crack lengths from the measured compliance of the specimen and independent measurements of the flexural modulus, E_1, rather than visually measuring crack lengths (see [39] for details of the calculations). Using this method for the determination of crack lengths would facilitate fatigue delamination measurements on FRP because after starting the test it would only be necessary to stop the test when a sufficiently low crack growth rate is reached. Simultaneously, possible shifts in machine data recording from stopping and restarting the fatigue loading and operator dependent visual determination of delamination length would be eliminated. Effective crack lengths, a_{eff}, were calculated via equation (3), which is derived from corrected beam theory:

$$a_{eff} = \frac{h}{2} \left(\frac{E_1 C b}{N} \right)^{\frac{1}{3}} \tag{3}$$

where h is half the thickness of the specimen, E_1 the flexural modulus, b the width of the specimen and N a finite displacement correction to account for load-block effects. The flexural moduli of materials A and B were measured on a tensile testing machine (type Zwick Roell Z250) with

a 10 kN load cell in laboratory A according to [40] while the value for material C was obtained from [41].

2.4 Calculation of da/dN

The crack growth rate, da/dN, was calculated using a seven point averaging method as described in ASTM E 647 [42]. This is an incremental polynomial method fitting a second order polynomial (parabola) to sets of (2n+1) successive data points, where n is 1, 2 or 3. The first and last pair of data points are evaluated using the secant or 2 point technique, where two points are connected with a straight line and the crack growth rate is the slope of this line. In order to examine a possible influence of the number of fitted data points on the calculation of da/dN the authors also calculated da/dN by using this 2 point technique and a 5 point technique, where n=2. With the aim of reducing the scatter in the compliance based calculation of da/dN observed in the first round robin [36] and illustrated in Fig. 1b, two approaches were selected. The first is to eliminate all data points which do not correspond to a delamination length increase of more than 0.1 mm (see Fig. 1c). The second uses a second order power law fit of the crack lengths calculated from compliance, which is plotted versus cycle number (see Fig. 1d).

2.5 Calculation of the strain energy release rate

The strain energy release rate in mode I, G_I, can also be calculated in various ways. The simplest method is to calculate it using so-called “simple beam theory” (SBT), see equation (4).

$$G_I = \frac{3P\delta}{2ba} \tag{4}$$

where P is the load and δ is the displacement. Since [34] recommends the use of corrected beam theory (CBT, see equation 5) and modified compliance calibration (MCC, see equation 6) for the calculation of G_I, these two calculation methods are also evaluated in this paper.

$$G_I = \frac{3P\delta}{2b(a+|\Delta|)} \tag{5}$$

where Δ is a correction factor to account for the effects of transverse shear and for deformation beyond the crack tip [43].

$$G_I = \frac{3m}{2(2h)}\left(\frac{P}{b}\right)^2\left(\frac{bC}{N}\right)^{2/3}F \tag{6}$$

where m is the slope of the linear fit of $(bC/N)^{1/3}$ over (a/2h) and F is a correction factor to account for large displacements and N the load-block correction [34, 44].

3 Results and Discussion

Figure 2 shows the results of all laboratories using the visually observed crack lengths for the determination of the crack growth rate, da/dN. The strain energy release rate was calculated via (a) SBT, (b) CBT and (c) MCC. In case of material A, taking all data from all laboratories into account, the inter-laboratory scatter of the data calculated via SBT is within about two decades of the crack growth rate. The in-laboratory scatter for the different labs is comparable and also amounts to about two decades in da/dN. When using compliance based methods for the calculation of the strain energy release rate, namely CBT and MCC, the scatter increases and can even reach up to two-and-one-half decades in da/dN. A factor that can play a role in the compliance based analysis schemes is the development of the fracture process zone with increasing number of fatigue cycles. Starting cyclic fatigue from a relatively short (a

few mm), quasi-static mode I precrack (a few mm long) may, depending on the type of composite, not necessarily correspond to starting from a steady-state crack tip with fully developed fracture process zone. Increasing the fracture process zone in the wake of the delamination tip can affect the compliance of the specimens.

The slope of the Paris plot, which is described by the exponent m (see equation 7) agrees fairly well for laboratories A, B, C, D and E in the da/dN-range between 10^{-3} and 10^{-6} mm/cycle for data calculated from visually observed crack lengths (see Figure 3a). The level for valid fits was arbitrarily defined by requiring a value for the coefficient of determination R^2 above 0.95. The results of laboratories D and E show significant scatter in the values of m and therefore contribute significantly to the inter-laboratory scatter of up to two-and-one-half decades (see Figures 2a, b and c).

$$\frac{da}{dN} = A \cdot G_{\mathrm{I}max}{}^{m} \tag{7}$$

For material B the in-laboratory and inter-laboratory scatter in da/dN in the Paris plot is larger than for material A, but similar for all participating labs. One of the causes of this increase in scatter is the partly unstable delamination behavior of material B. The crack did not grow continuously, but showed stochastic arrest effects. This has an influence on the linearization of a compliance based term over a crack length based term in both CBT and MCC. Again the scatter clearly increases when compliance based methods (namely CBT and MCC) were used to calculate G_{Imax}, this time going up from one-and-one-half decades to several decades in da/dN.

The variation in slope for Material B in the case of visually observed crack lengths can be seen in Figure 3b. While data from laboratory D yielded results with the highest values for m, laboratory E did not deliver valid data at all (R^2>0.95). The average value from the valid round robin data of 8.63 is higher than that of 6.14 determined by [18]. However, literature data cited in [18] cover a range of slopes between 3.0 and 10.5, i.e., an apparent inter-laboratory scatter of roughly ±3, i.e. comparable with the ±2.28 found in the present round robin. The larger scatter observed in the position of the Paris plot on the G_{Imax} axis for material B, on the other hand, makes it questionable whether such data can be used in design (unless unrealistically large safety factors are applied).

Figure 4 shows the course of da/dN over G_{Imax} values calculated with MCC from pairs of load and displacement data via the compliance based crack length approach. Compared to the graphs shown in Figure 2, and specifically Fig. 2a with crack length from visual observation, the scatter is larger than any of these types of G_{Imax} calculation. This indicates that the use of compliance data for the calculation of either da/dN or G_{Imax} is directly responsible for the scatter in the plots. Since compliance is calculated from displacement and load which are machine parameters influenced by test set-up, it is important to use a sufficiently stiff test machine, a load cell within a load range just above the maximum loads appearing in the test (in this case about 500N) and preferably local displacement measurements (e.g. clip on extensometers). Asp et al. [23] carried out cyclic delamination tests on HTA/6376C and used a 250N load cell range. Still, the scatter in the da/dN versus G_{Imax} curve was roughly one decade of da/dN. Figures 5a and 5b and Tables 2 and 3 again show values for the slopes of the Paris plots, for material A and B, respectively,

in this case for the results calculated via the compliance based crack length approach. The values agree quite well with those calculated from visually observed crack lengths in Figures 3a and 3b. Only one valid fit (R^2>0.95) could be generated with data from laboratory D for both material A and B. The same holds for material B of laboratory E. Tables 2 and 3 show values of the exponent m (see equation 7) for power law fits of Paris plots for materials A and B respectively. Two types of da/dN calculation are compared. 7 point fitting as described in [42] and fitting of crack length data with a second order power law fit as described above. All data that was calculated via the latter route was further refined by setting an arbitrary limit for the coefficient of determination (R^2) of 0.95. All data that did not meet this criterion was rejected. Thereby the in- and inter-laboratory scatter of the slope values could be greatly reduced. In both cases the scatter of the slope value increases when using compliance based methods to calculate the strain energy release rate.

In Figure 6 the Paris plots for the case of crack lengths calculated via the effective crack length approach are shown. The flexural modulus for the determination of the effective crack length was measured on 10 specimens for each material. E_1 amounted to 118±7 GPa for material A, to 120±6 GPa for material B and to 120±2 GPa for material C [41]. In contrast to the results shown above (Fig.2c and Fig.4, i.e., crack length determined from visual observation and compliance measurements) the results calculated via MCC and a_{eff} show less scatter. No clear explanation can be given for this phenomenon.

Figure 7 directly compares the results of SBT, CBT and MCC for one laboratory. The crack growth rates were calculated from visually observed crack lengths, crack lengths calculated via compliance calibration and

crack lengths calculated via the effective crack length method. The different crack length calculation methods seem to agree quite well with respect to the resulting slope in the Paris plot, but the SBT data seem to be shifted in either da/dN or G_{Imax} relative to those from CBT or MCC. MCC and CBT, therefore, show more conservative values than SBT. In the low delamination growth rate regime increasing scatter can be seen. In order to evaluate the source of this scatter, a load trace is plotted in Figure 8a. It can be seen, that the loads rapidly decrease to below 30 N. In Figure 8b the influence of the da/dN averaging method on Paris plots of CFRPs with epoxy matrix is shown. Four types of da/dN calculation were used. For the secant method (2 point method) da/dN was calculated from the slope of a line connecting two adjacent value pairs of crack length and number of cycles. With the 5-point and 7-point polynomial fitting method, respectively, da/dN was calculated by fitting a second order polynomial to sets of 5 and 7 successive data points [42]. The fourth type of da/dN calculation included a second order power law fit of the crack length data obtained from compliance calibration versus number of cycles and numerical differentiation of this fit function. It can be seen that the averaging technique has an effect on the values of da/dN and that the power law fit results in the smoothest curves.

In Figure 9a crack lengths calculated from various approaches (see section 2.3) and the corresponding load signal are plotted versus number of cycles. Crack lengths calculated via compliance calibration seem to agree quite well with visually measured crack lengths. The effective crack length approach yields lower values. This difference may possibly be explained by the use of the average E-modulus value rather than the individual modulus of the specimen used.

When da/dN is calculated from the compliance data calculated from this load signal via the 7-point method without prior data reduction, then a considerable amount of scatter in da/dN is received, see Figure 9b. This scatter can be caused even by very little scatter in the load trace, since it is transferred to crack length data when calculating crack lengths via compliance. One way to reduce this scatter is deleting data that does not meet a minimum increment of 0.1 mm in crack length, see Figure 9c. However, even with this filter, every spike in the compliance data can lead to scatter in the da/dN data. When fitting the full range of load data with a second-order power law the least scatter in da/dN is received, see Figure 9d. Applying this procedure to the calculation of the Paris plots yields Figure 10. The scatter for both materials is clearly reduced when compared to that from the other analysis methods including polynomial fitting and now amounts to much less than the two decades or more seen in the raw data (compare Figs. 2, 4 and 6).

It can be questioned whether the fitting and numerical differentiation procedure for machine load data presented above as an alternative approach for improving Paris plots of mode I delamination fatigue (da/dN versus G_{Imax}) with respect to in- and inter-laboratory scatter will not mask incipient changes towards a threshold behavior with increasing number of fatigue cycles. In order to investigate this, selected crack length versus number of cycles data were fitted within incremental ranges (20%, 40%, 60%, 80%) of the full data set and compared with the “full” fit of the complete recorded data (100%). These fits, extrapolated to the full number of tested cycles are shown in Figure 11a. It can be seen that, at least in this example, the extrapolation of the fit of the first 20% of the crack length data clearly over-estimates the effectively observed crack length (starting

at less than 100’000 cycles). The other fits yield roughly comparable extrapolations. Figure 11b then shows the error in crack length for the different extrapolations compared with the “full” power law fit of all recorded data. In this case, the 60%-fit does slightly over- and the 40% and 80%-fits slightly under-estimate the crack length from the “full” fit. The errors in this case are on the order of 0.05 to 0.07 mm, i.e., about at the level of resolution required for delamination length measurements in [34]. The preliminary analysis presented here at least supports the interpretation that it is unlikely that the “full” fit will “hide” clear trends towards a threshold behavior. The only source for an apparent threshold behavior in the round robin data identified so far, therefore, remains the scatter in recorded load data (when testing under displacement control) [38].

Since materials A and B, used in ESIS TC4 round robin 2, were stored for several years under laboratory conditions, the influence of the strain energy release rate calculation on the course of da/dN over G_{Imax} was additionally investigated with material C, which was a newly manufactured material tested in ESIS TC4 round robin 1 in 2008 and 2009. The results are compared with those of materials A and B in Figure 12. Again, the results generated by CBT and MCC show more conservative values than SBT. Nevertheless it has to be considered that MCC and CBT can result in more scatter than SBT as shown in Figure 2. The combination of more conservative values and larger scatter will ultimately yield more conservative limits when using fracture mechanics based structural design.

4 Conclusions

In this paper the results of a mode I fatigue delamination round robin with three carbon fiber-reinforced laminates performed at five different laboratories are compared.

The inter-laboratory scatter of the raw data is significant (amounting to more than two decades in delamination propagation da/dN for a given value of G_{Imax}) and depends on the type of laminate (less for CF-Epoxy than for CF-PEEK). It may hence be questioned whether the data can be used in fracture mechanics based structural design. Detailed investigation has shown that even small scatter in the recorded load signal (when testing under displacement control) can yield significant in- and inter-laboratory scatter. Smoothing data with polynomial fitting according to [42] and/or using a load cell range with high resolution (0-500N or 0-200N) are shown to be less effective in reducing scatter than a second order power law fit and numerical differentiation of the load versus cycle number signal. Detailed analysis of the slope “m” of the linear part of the Paris plot determined by linear fitting further seem to indicate that operator experience may affect the observed scatter as well. Introducing a quantitative, but arbitrary, criterion for the correlation coefficient (R^2 >0.95) for the slope fitting, combined with power law fitting of the load signal approach yielded in- and inter-laboratory scatter in the linear part of the Paris plots (da/dN versus G_{Imax}) on the order of 1.5 decades in da/dN for material A and less than one decade in da/dN for material B for a given value of G_{Imax} or, alternatively, a scatter of less than ±3 in the average slope for material A and less than ±2 for material B. The range of materials, participating test laboratories and test machines used in the round robins makes it rather unlikely that further significant reductions in

scatter will be feasible, unless other test procedures (e.g., operator-independent delamination length approach [39]) or more sophisticated data fitting algorithms are used.

Comparing different data analysis schemes (simple and corrected beam theory, modified compliance calibration) indicates that the latter two yield more conservative results than simple beam theory, but also somewhat higher scatter. Design rules considering scatter-based safety factors may hence result in more conservative designs if data analysis uses corrected beam theory or modified compliance calibration.

The results obtained in the round robins, the range of test equipment, test parameters and composite materials explored so far as well as the elucidation of effects that contribute to scatter and how these are affected by different averaging procedures now provide a solid basis for drafting a standard test and analysis procedure for mode I fatigue delamination propagation.

5 Acknowledgments

The experimental technical assistance provided by Mr. Daniel Völki (Empa) and Dr. Joseph Mohan (UCD) and helpful discussions with Dr. James G. Ratcliffe and Dr. William M. Johnston (National Institute of Aerospace, USA) are gratefully acknowledged.

6 References

[1] Shue B, Moreira A, Flowers G. Review of recent developments in composite material for aerospace applications: Presented at 2009 ASME International Design Engineering Technical Conferences and Computers and Information in Engineering Conference, August 30 - September 2, 2009, San Diego, California USA. Proceedings of the

ASME International Design Engineering Technical Conferences and Computers and Information in Engineering Conference 2009 2010:811–9.

[2] Gloria A, Ronca D, Russo T, D'Amora U, Chierchia M, Santis R de et al. Technical features and criteria in designing fiber-reinforced composite materials: from the aerospace and aeronautical field to biomedical applications. Journal of Applied Biomaterials and Biomechanics 2011;9(2):151–63.

[3] Gibson RF. A review of recent research on mechanics of multifunctional composite materials and structures. Composite Structures 2010;92(12):2793–810.

[4] Gorbatikh L, Lomov SV, Verpoest I. Nano-engineered composites: a multiscale approach for adding toughness to fibre reinforced composites. Procedia Engineering 2011;10:3252–8.

[5] Tay TE. Characterization and analysis of delamination fracture in composites: An overview of developments from 1990 to 2001. Applied Mechanics Reviews 2003;56:1–31.

[6] Brunner AJ, Blackman BRK, Davies P. A status report on delamination resistance testing of polymer–matrix composites. Engineering Fracture Mechanics 2008;75(9):2779–94.

[7] Williams JG. On the calculation of energy release rates for cracked laminates. International Journal of Fracture 1988;36:101–19.

[8] Williams JG. The fracture mechanics of delamination tests. Journal of Strain Analysis for Engineering Design 1989;24(4):207–14.

[9] Newaz GM, Ahmad J. A simple technique for measuring mode I delamination energy release rate in polymeric composites. Engineering Fracture Mechanics 1989;33(4):541–52.

[10] O'Brien TK, Roderick H. Martin. Round robin testing for mode I interlaminar fracture toughness of composite materials. Journal of Composites Technology & Research 1993;15(4):269–81.

[11] Hojo M, Kageyama K, Tanaka K. Prestandardization study on mode I interlaminar fracture toughness test for CFRP in Japan. Composites 1995;26:243–55.

[12] Martin R. Interlaminar Fracture Characterization. Key Engineering Materials) 1996;120-121:329–46.

[13] O'Brien TK. Interlaminar fracture toughness: the long and winding road to standardization. Composites Part B: Engineering 1998;29(1):57–62.

[14] Hojo M, Tanaka K, Gustafson CG, Hayashi R. Effect of stress ratio on near-threshold propagation of delamination fatigue cracks in unidirectional CFRP. Composites Science and Technology 1987;29:273–92.

[15] Adams DF, Zimmerman RS, Odom EM. Frequency and load ratio effects on critical strain energy release rate G_c thresholds of graphite/epoxy composites. In: Johnston NJ, editor. Toughened Composites: ASTM STP 937. West Conshohocken, PA: American Society for Testing and Materials; 1987, p. 242–259.

[16] O'Brien TK. Fatigue delamination behavior of PEEK thermoplastic composite laminates. Journal of Reinforced Plastics and Composites 1988;7:341–59.

[17] Newaz GM, Mall S. Relaxation-Controlled Cyclic Delamination Growth in Advanced Thermoset and Thermoplastic Composites at Elevated Temperature. Journal of Composite Materials 1989;23(2):133–45.

[18] Martin RH, Murri GB. Characterization of mode I and mode II delamination growth and thresholds in AS4/PEEK composites. In: Garbo S, editor. Composite Materials: Testing and Design: ASTM STP 1059. West Conshohocken, PA: American Society for Testing and Materials; 1990, p. 251–270.

[19] Dahlen C, Springer GS. Delamination growth in composites under cyclic loads. Journal of Composite Materials 1994;28(8):732–81.

[20] Hojo M, Ochiai S. Effect of matrix resin on delamination fatigue crack growth in CFRP laminates. Engineering Fracture Mechanics 1994;49(1):35–47.

[21] Cvitkovich M. Polymer matrix effects on interlaminar crack growth in advanced composites under monotonic and fatigue mixed-mode I/II loading conditions. Ph.D. Thesis. Leoben; 1995.

[22] Martin RH. Delamination characterization of woven glass/polyester composites. Journal of Composites Technology & Research 1997;19(1):20–8.

[23] Asp LE, Sjorgen A, Greenhalgh ES. Delamination growth and thresholds in a carbon/epoxy composite under fatigue loading. Journal of Composites Technology & Research 2001;23(2):55–68.

[24] Hojo M, Ando T, Tanaka M, Adachi T, Ochiai S, Endo Y. Modes I and II interlaminar fracture toughness and fatigue delamination of CF/epoxy laminates with self-same epoxy interleaf. International Journal of Fatigue 2006;28(10):1154–65.

[25] Argüelles A, Viña J, Canteli AF, Bonhomme J. Fatigue delamination, initiation, and growth, under mode I and II of fracture in a carbon-fiber epoxy composite. Polym. Compos 2009:700–6.

[26] Martin RH. Incorporating interlaminar fracture mechanics into design. Proceedings of the Institution of Mechanical Engineers, Part L: Journal of Materials Design and Applications 2000;214(2):91–7.

[27] Murri GB, Schaff JR. Fatigue life methodology for tapered hybrid composite flexbeams. Composites Science and Technology 2006;66(3-4):499–508.

[28] Shivakumar K, Chen H, Abali F, Le D, Davis C. A total fatigue life model for mode I delaminated composite laminates. International Journal of Fatigue 2006;28(1):33–42.

[29] Wimmer G, Pettermann H. A semi-analytical model for the simulation of delamination in laminated composites. Composites Science and Technology 2008;68(12):2332–9.

[30] Wimmer G, Schuecker C, Pettermann H. Numerical simulation of delamination in laminated composite components – A combination of a strength criterion and fracture mechanics. Composites Part B: Engineering 2009;40(2):158–65.

[31] Chen J, Ravey E, Hallett S, Wisnom M, Grassi M. Prediction of delamination in braided composite T-piece specimens. Composites Science and Technology 2009;69(14):2363–7.

[32] JIS - Japanese Standards Association. JIS K 7086:1993 Testing methods for interlaminar fracture toughness of carbon fibre reinforced plastics(K 7086); 1993.

[33] ASTM - American Society for Testing and Materials. ASTM D5528:2001 - Standard test method for mode I interlaminar fracture toughness of unidirectional fiber-reinforced polymer matrix composites.

[34] ISO - International Organization for Standardization. ISO 15024:2001 - Fibre-reinforced plastic composites — Determination of mode I interlaminar fracture toughness, GIC, for unidirectionally reinforced materials.

[35] ASTM - American Society for Testing and Materials. ASTM D6115:1997 - Standard test method for mode I fatigue delamination growth onset of unidirectional fiber-reinforced polymer matrix composites.

[36] Brunner AJ, Murphy N, Pinter G. Development of a standardized procedure for the characterization of interlaminar delamination propagation in advanced composites under fatigue mode I loading conditions. Engineering Fracture Mechanics 2009;76(18):2678–89.

[37] Brunner AJ, Paris I, Pinter G. Fatigue propagation test development for polymer-matrix fibre-reinforced laminates. Proc. 12th Int. Conf. on Fracture ICF-12, paper No. 00371 2009;1-8 2009:1–8.

[38] Stelzer S, Brunner AJ, Argüelles A, Murphy N, Pinter G. Mode I delamination fatigue crack growth in unidirectional fiber reinforced composites: Development of a standardized test procedure. Composites Science and Technology 2012;72(10):1102–7.

[39] Brunner AJ, Blackman BRK, Williams JG. Calculating a damage parameter and bridging stress from GIC delamination tests on fibre composites. Composites Science and Technology 2006;66(6):785–95.

[40] ISO - International Organization for Standardization. ISO 178:2010 - Plastics - Determination of flexural properties.

[41] Bamber Blackman. (Imperial College London) private communication.

[42] ASTM - American Society for Testing and Materials. ASTM E647:2011 - Standard test method for measurement of fatigue crack growth rates; 2011.

[43] Williams JG. End corrections for orthotropic DCB specimens. Composites Science and Technology 1989;35:367–76.

[44] Kageyama K, Kobayashi T, Chou T. Analytical compliance method for mode I interlaminar fracture toughness testing of composites. Composites 1987;18(5):393–9.

Figures

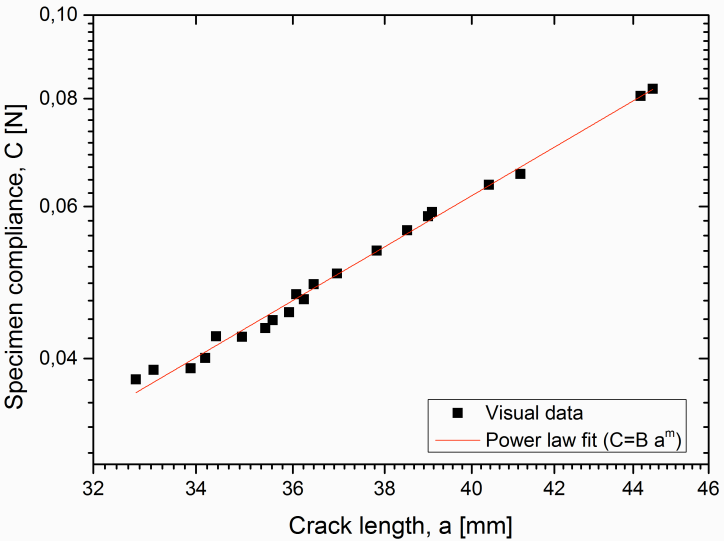

(figure 1a)

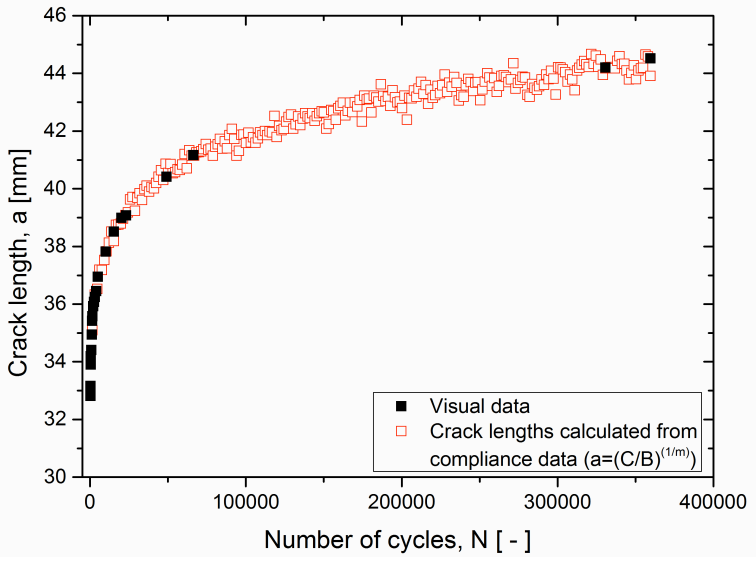

(figure 1b)

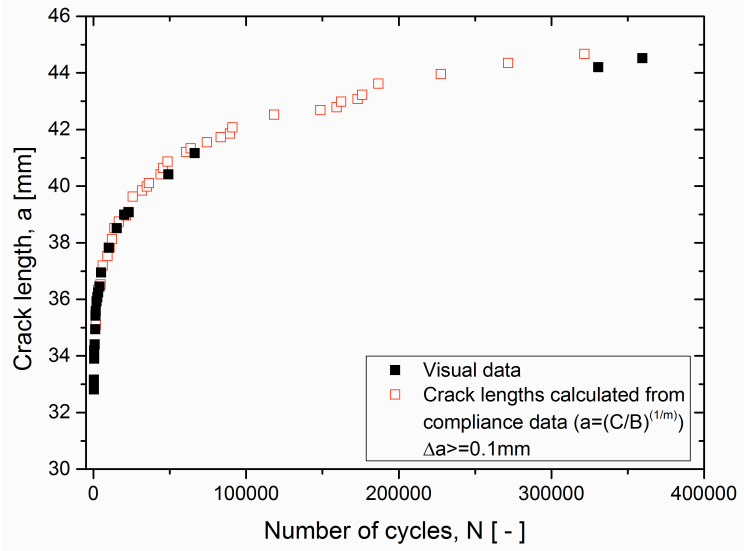

(figure 1c)

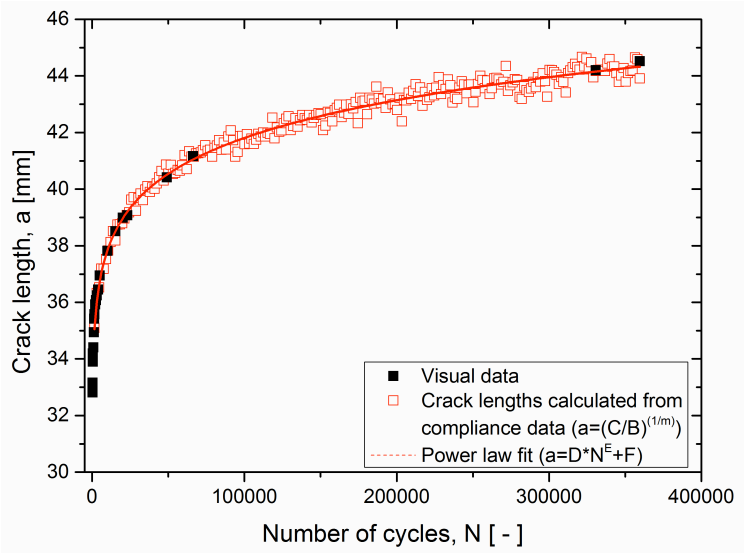

(figure 1d)

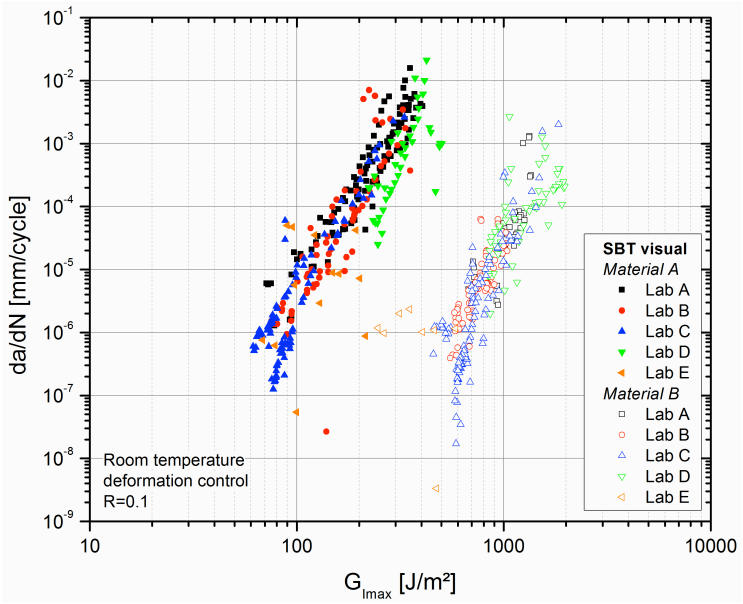

(figure 2a)

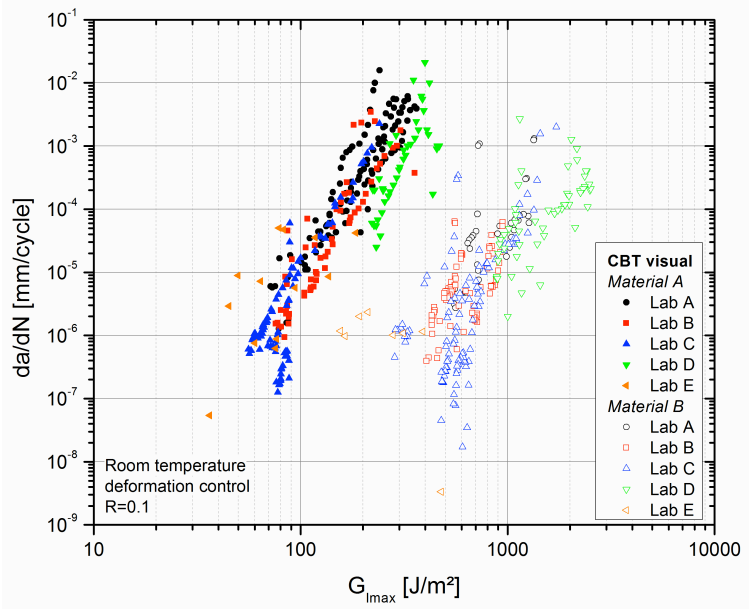

(figure 2b)

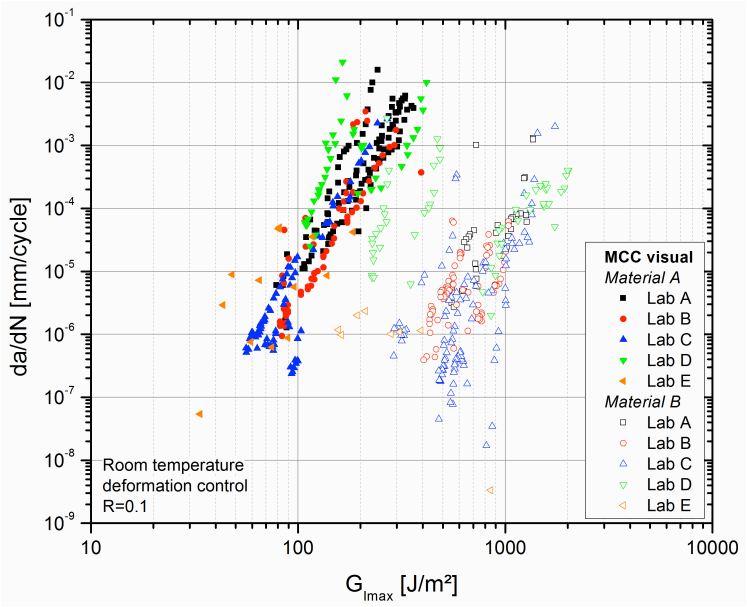

(figure 2c)

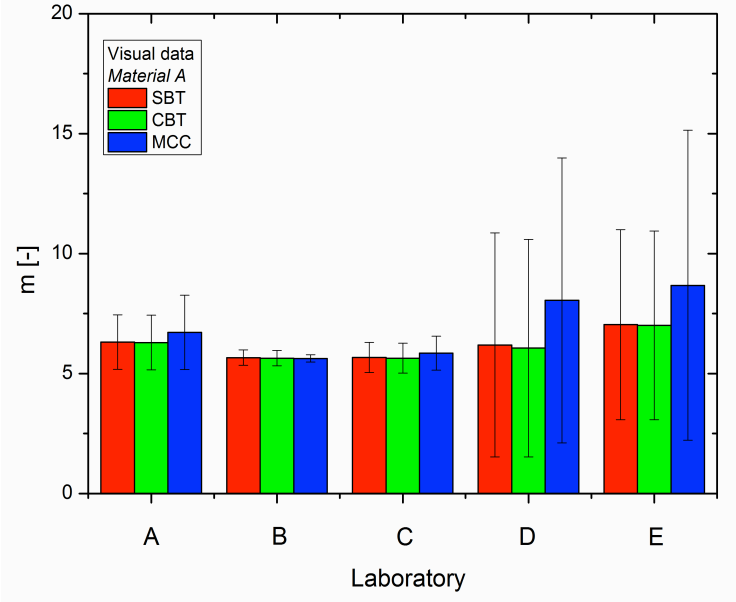

(figure 3a)

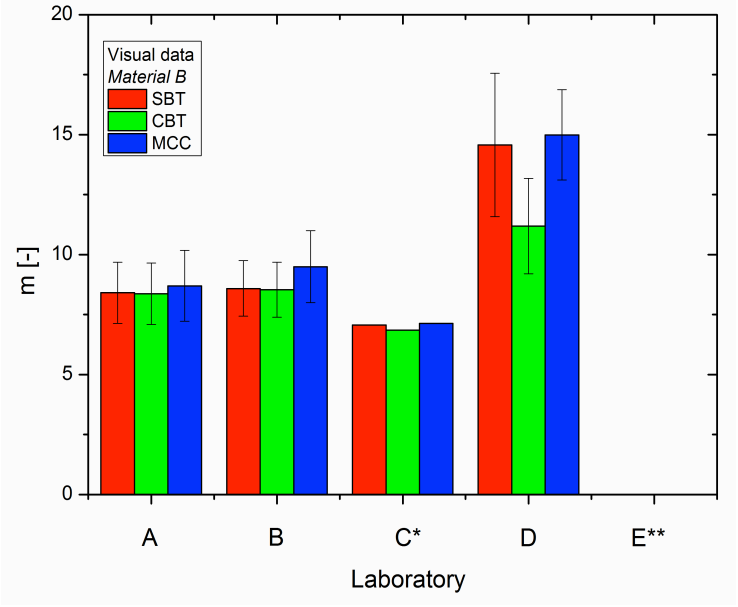

(figure 3b)

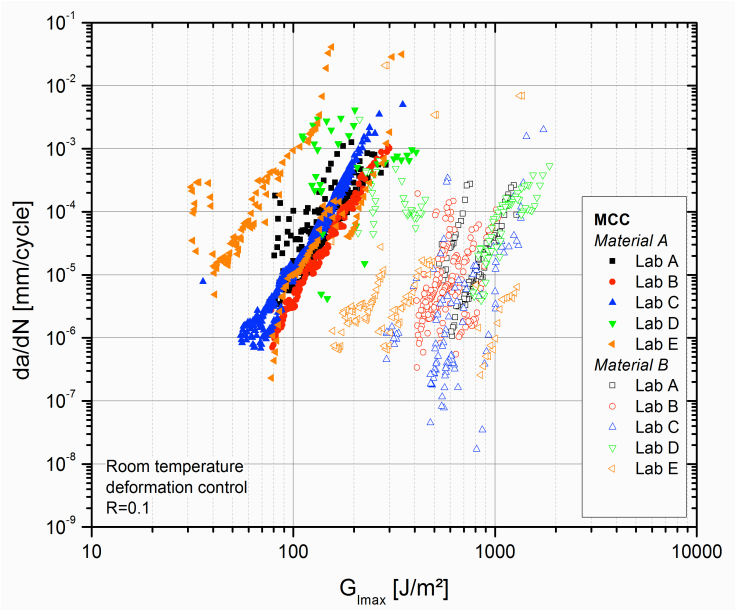

(figure 4)

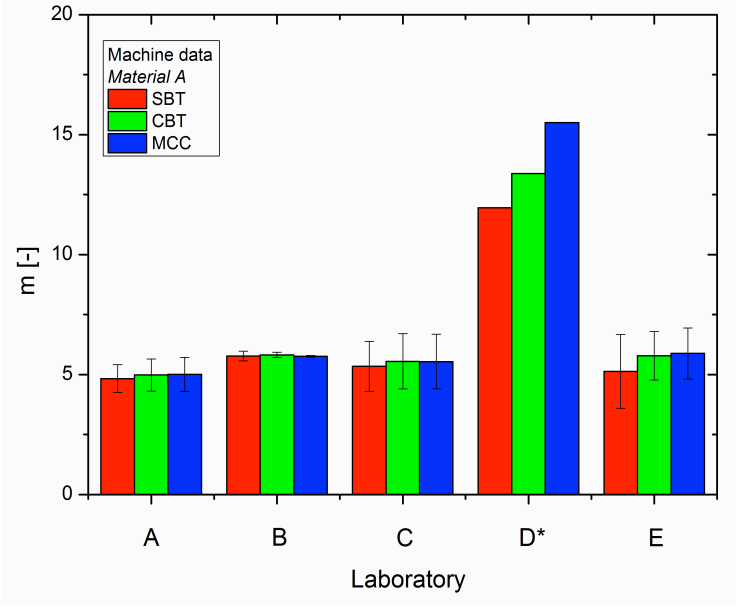

(figure 5a)

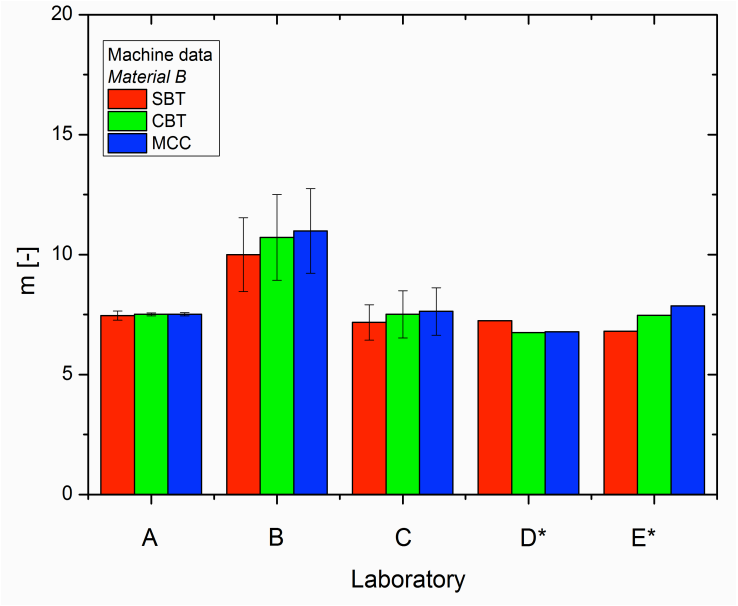

(figure 5b)

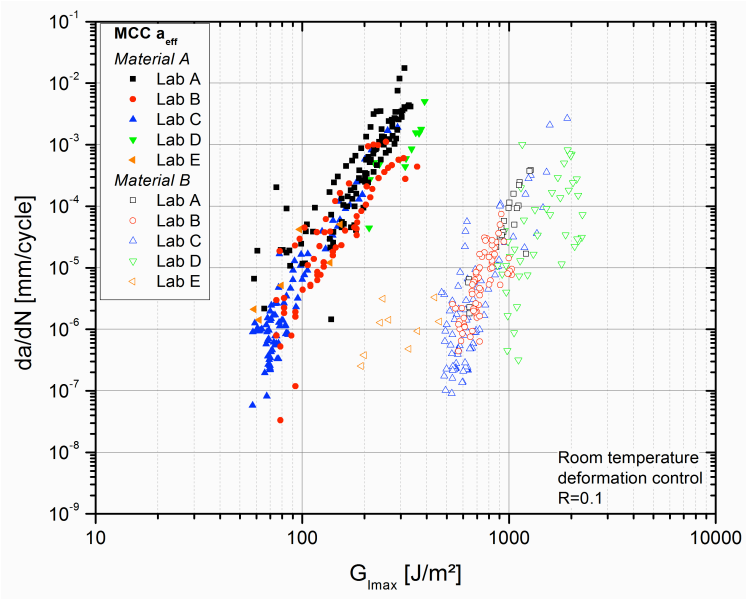

(figure 6)

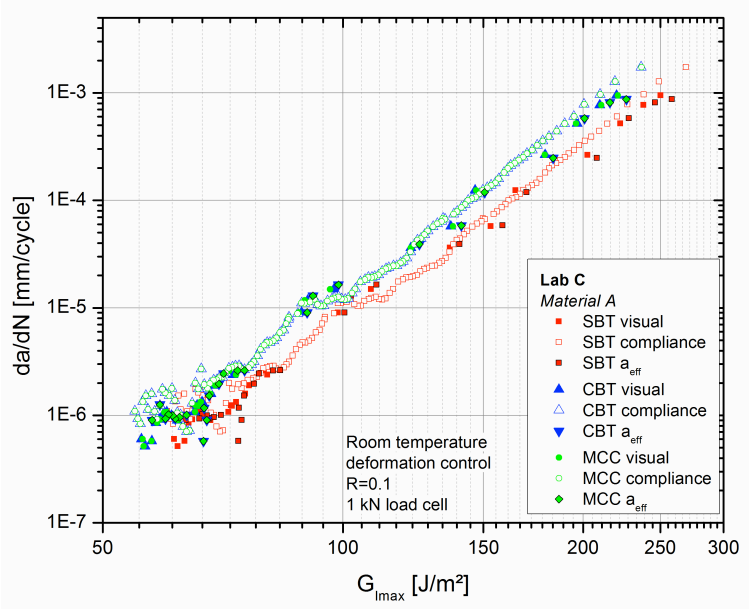

(figure 7)

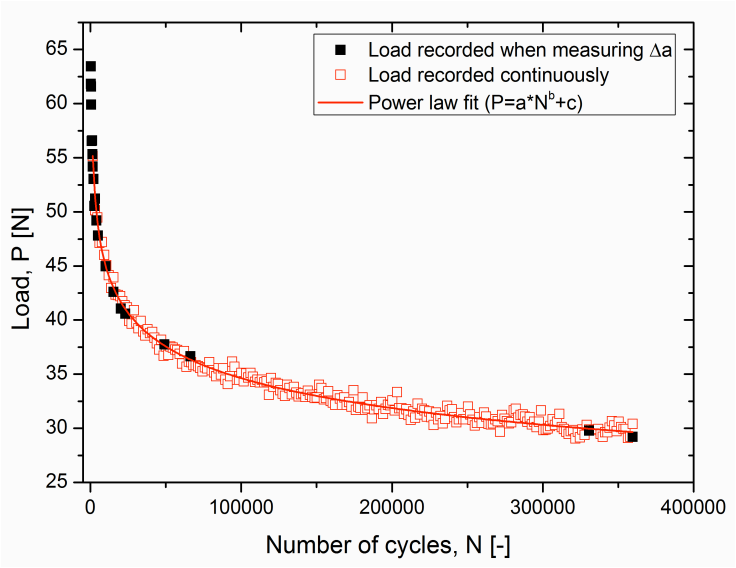

(figure 8a)

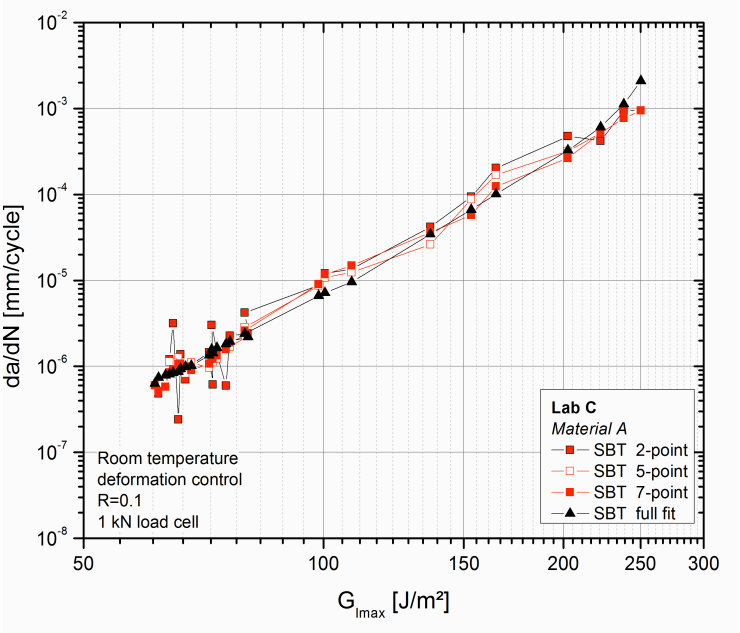

(figure 8b)

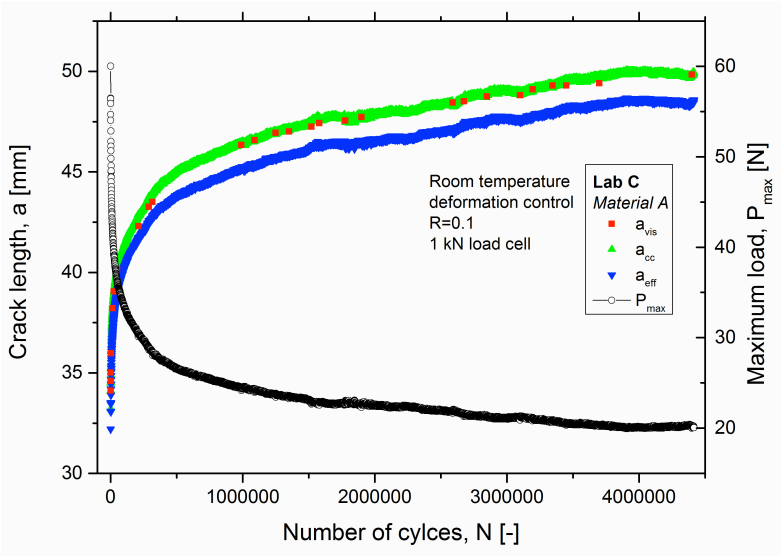

(figure 9a)

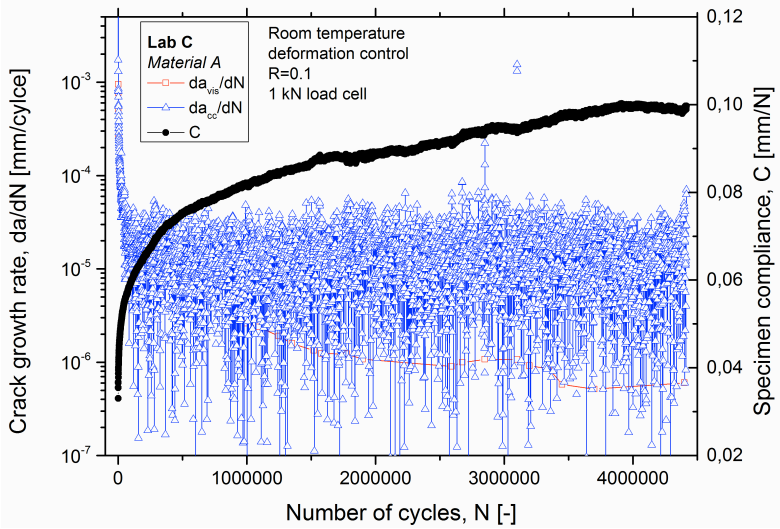

(figure 9b)

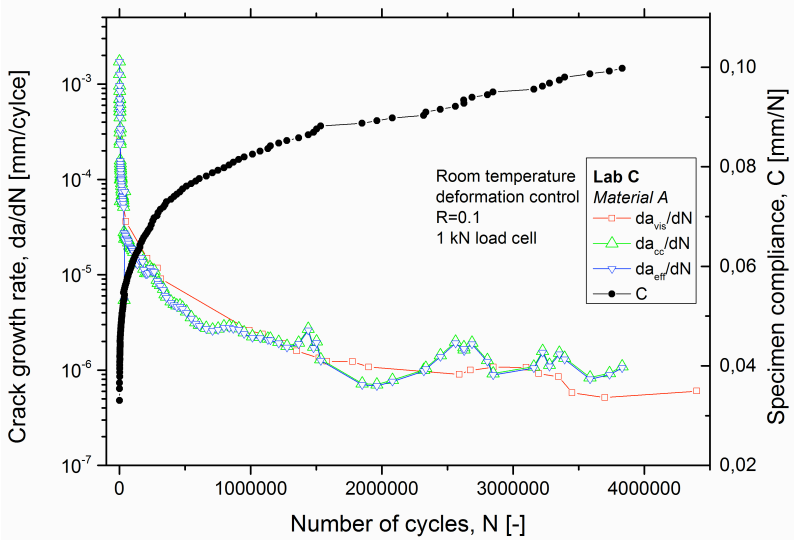

(figure 9c)

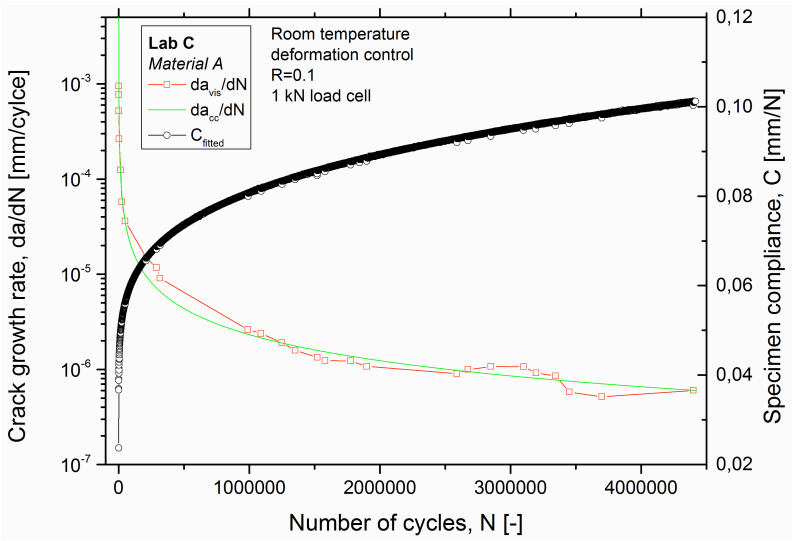

(figure 9d)

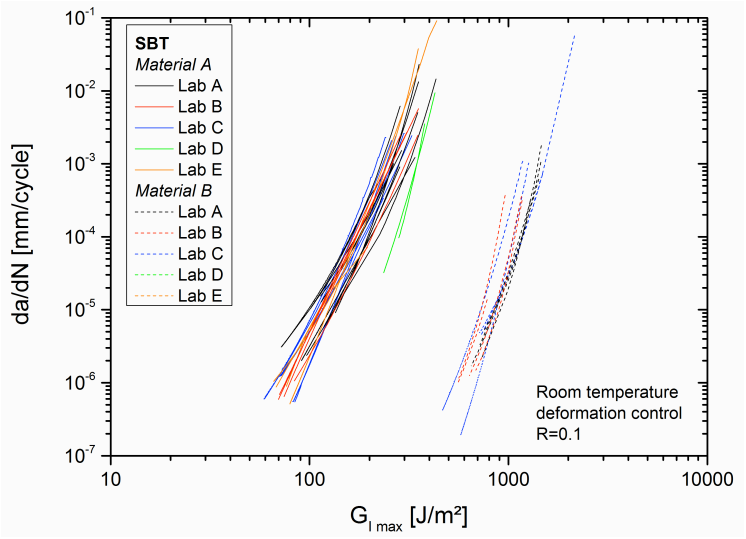

(figure 10)

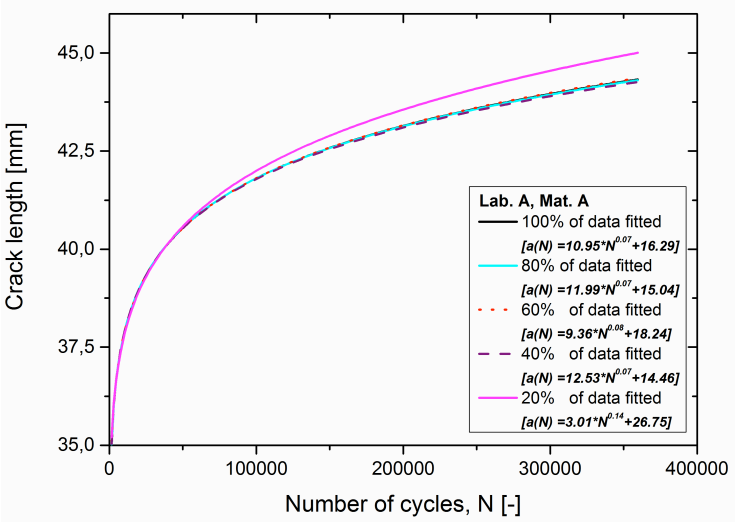

(figure 11a)

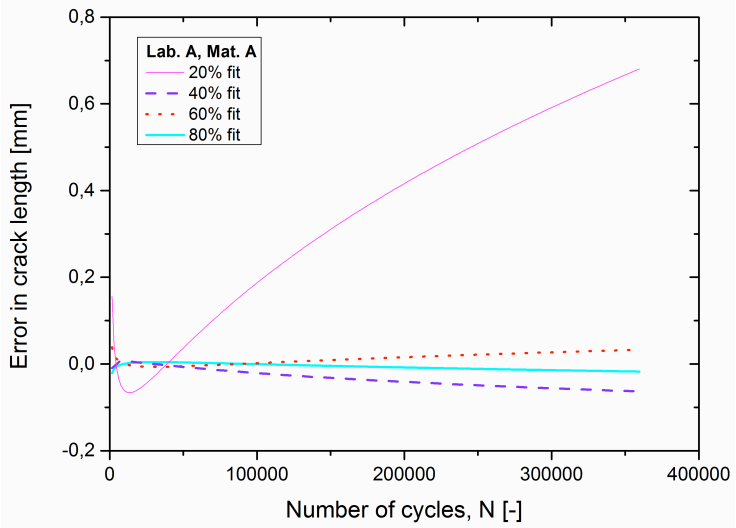

(figure 11b)

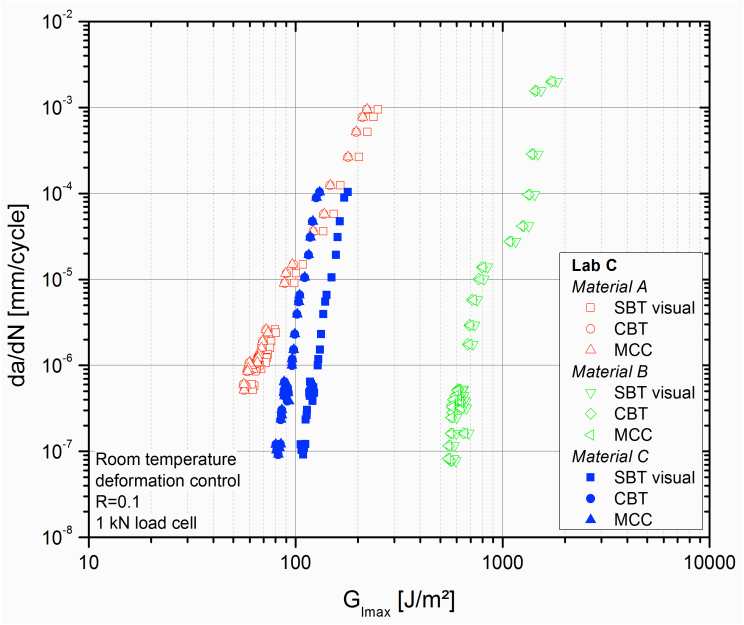

(figure 12)

Figure Captions

Figure 1: Calculation of crack lengths from load and displacement data recorded by the test machine (Lab A and material A).

(a) Correlation between specimen compliance and visually measured crack lengths.

(b) Visually measured crack lengths and crack lengths calculated from compliance data versus number of cycles.

(c) Visually measured crack lengths and crack lengths calculated from compliance data versus number of cycles after data reduction ($\Delta a > 0.1$ mm).

(d) Visually measured crack lengths, crack lengths calculated from compliance data and a fit of crack lengths calculated via compliance.

Figure 2: Paris plots from visually observed crack lengths.

(a) Paris plots with G_I calculated via simple beam theory.

(b) Paris plots with G_I calculated via corrected beam theory.

(c) Paris plots with G_I calculated via modified compliance calibration.

Figure 3: Slopes m of the Paris plots (visually measured crack lengths). The data were fitted with a power law relationship as shown in equation (8). All fits that did not meet an arbitrary minimum R^2 of 0.95 were rejected.

(a) Values of exponent m for material A.

(b) Values of exponent m for material B.

* ..... Fit for only one specimen. For all other specimens the value of determination of the fits was too low.

** ..... No valid fits could be created for data of laboratory E.

Figure 4: Paris plots from crack lengths calculated via compliance calibration. Paris plots with G_I calculated via modified compliance calibration

Figure 5: Slopes m of the Paris plots (crack lengths calculated from compliance data). The data were fitted with a power law relationship as shown in equation (8). All fits that did not meet a minimum R^2 of 0.95 were rejected.

(a) Values of exponent m for material A.

(b) Values of exponent m for material B.

* ..... fit for only one specimen. For all other specimens the value of determination of the fits was too low.

Figure 6: Paris plots. Crack growth rates calculated from effective crack lengths and G_{Imax} calculated via modified compliance calibration.

Figure 7: Influence of different G_{Imax} calculation methods on the Paris plots of materials A, B and C.

Figure 8: (a) Load versus number of cycles.

(b) Influence of da/dN averaging method on the Paris plot.

Figure 9: Influence of processing of compliance data on scatter in da/dN.

(a) Crack length and maximum Load, P_{max}, versus number of cycles.

a_{vis} .. visually measured crack length

a_{cc} ... crack length calculated via compliance calibration

a_{eff}... effective crack length

(b) Specimen compliance, C, and crack growth rate, da/dN, versus number of cylces. All da/dN values calculated via 7-point method.

(c) Specimen compliance and da/dN values after eliminating all compliance data that do not meet the $\Delta a > 0.1$ mm criterion.

(d) Course of specimen compliance fitted with a second order polynomial and resulting da/dN curve.

Figure 10: Paris plots of data calculated via the path described in Fig. 9d.

Figure 11: Influence of fitting range on quality of the fit.

(a) Fits of 20, 40, 60, 80 and 100% of the full range of crack length data calculated from compliance.

(b) Error of extrapolated fits (20, 40, 60 and 80% of full range data fitted) compared to a fit of the full range data.

Figure 12: Comparison of different averaging methods for the calculation of the crack growth rate da/dN.

(a) material A

(b) material B

(c) material C

Tables

Table 1: Materials used in the ESIS TC4 round robins.

	A	**B**	**C**
Fiber	Carbon, G30-500 12k	Carbon, AS4	Carbon, IM7
Matrix resin	Epoxy, Rigidite 5276	PEEK	Epoxy, 977-2
Lay-up	[0]	[0]	[0]
Thickness (mm)	4.0	3.0	4.0
Starter film type and thickness	PTFE, 20 µm	PTFE, 20 µm	FEP, 10 µm

Table 2: Slope values obtained from fits of Paris plots of material A. All results calculated from machine data. Values for standard deviations in brackets.

Strain energy release rate calculation		Simple Beam Theory		Corrected Beam Theory		Modified Compliance Calibration	
da/dN calculation		7-point	full fit	7-point	full fit	7-point	full fit
Laboratory	A	4.17 (0.86)	4.83 (0.58)	4.32 (0.93)	4.98 (0.67)	4.30 (0.93)	5.01 (0.71)
	B	0.49 (6.72)	5.77 (0.20)	-6.67 (23.07)	5.82 (0.11)	-6.85 (23.48)	5.76 (0.03)
	C	3.69 (3.16)	5.34 (1.04)	3.85 (3.27)	5.55 (1.15)	4.04 (2.41)	5.54 (1.14)
	D	0.41 (3.06)	11.95*	0.40 (3.05)	13.38*	0.15 (3.27)	15.50*
	E	3.08 (2.13)	5.13 (1.54)	3.34 (2.34)	5.78 (1.01)	3.41 (2.22)	5.88 (1.06)
Mean value of all tests		2.46 (3.87)	5.65 (2.01)	0.87 (11.41)	5.99 (2.27)	0.83 (11.59)	6.17 (2.81)

* ..... Only one valid specimen (R^2>0.95)

7-point..... Seven point averaging method for the calculation of da/dN as described in ASTM E647 [42]

full fit ..... Fitting the full range of crack length data versus number of cycles with a second order power law fit

Table 3: Slope values obtained from fits of Paris plots of material B. All results calculated from machine data. Values for standard deviations in brackets.

Strain energy release rate calculation		Simple Beam Theory		Corrected Beam Theory		Modified Compliance Calibration	
da/dN calculation		7-point	full fit	7-point	full fit	7-point	full fit
Laboratory	A	7.57 (0.72)	7.46 (0.19)	7.92 (1.24)	7.51 (0.06)	7.92 (1.24)	7.51 (0.07)
	B	7.14 (2.67)	10.00 (1.54)	7.52 (2.73)	10.72 (1.79)	7.48 (2.68)	10.99 (1.76)
	C	9.47 (5.45)	7.17 (0.74)	10.35 (6.14)	7.51 (0.99)	10.94 (8.14)	7.63 (0.99)
	D	2.01 (4.69)	7.24*	1.81 (3.95)	6.75*	1.72 (4.45)	6.78*
	E	9.10 (5.71)	6.80*	6.09 (1.22)	7.47*	5.90 (1.42)	7.86*
Mean value of all tests		7.17 (4.79)	8.05 (1.58)	7.09 (4.75)	8.40 (1.89)	7.38 (5.85)	8.56 (1.95)

* ..... Only one valid specimen (R^2>0.95)

7-point..... Seven point averaging method for the calculation of da/dN as described in ASTM E647 [42]

full fit ..... Fitting the full range of crack length data versus number of cycles with a second order power law fit

Table Captions

Table 1: Materials used in the ESIS TC4 round robin.

Table 2: Slope values obtained from fits of Paris plots of material A. All results calculated from machine data. Values for standard deviations in brackets.

Table 3: Slope values obtained from fits of Paris plots of material B. All results calculated from machine data. Values for standard deviations in brackets.